NASA Technical Memorandum 88950

Elevated Temperature Tension, Compression, and Creep-Rupture Behavior of [001]-Oriented Single Crystal Superalloy PWA 1480

Mohan G. Hebsur and Robert V. Miner
Lewis Research Center
Cleveland, Ohio

February 1987

NASA

ELEVATED TEMPERATURE TENSION, COMPRESSION, AND CREEP-RUPTURE BEHAVIOR OF [001]-ORIENTED SINGLE CRYSTAL SUPERALLOY PWA 1480

Mohan G. Hebsur and Robert V. Miner
National Aeronautics and Space Administration
Lewis Research Center
Cleveland, Ohio 44135

E-3074

SUMMARY

Tensile and compressive flow behavior at various temperatures and strain rates, and tensile creep rupture behavior at 850 and 1050 °C and various stresses were studies for [001]-oriented single crystals of the Ni-base superalloy PWA 1480. At temperatures up to 760 °C, the flow stress is insensitive to strain rate and of greater magnitude in tension than in compression. At temperatures of 800 °C and above, the flow stress decreases continuously with decreasing strain rate and the tension/compression anisotropy diminishes.

The second stage creep rate and rupture time exhibited power law relationships with the applied stress for both 850 and 1050 °C, however with different stress dependencies. The stress exponent for the steady state creep rate was about 7 at 1050 °C, but much higher at 850 °C, about 12. Directional coarsening of the γ'-phase occurred during creep at 1050 °C, but not at 850 °C.

INTRODUCTION

Single crystal Ni-base superalloys containing a high volume fraction of the γ'-phase are currently being used as blades and vanes in advanced gas turbine engines because of their excellent resistance to stress and oxidation at high temperatures ($T > 0.5\ T_m$)(ref. 1). Turbine blades must resist high stresses (>600 MPa) at about 750 °C in the blade root and lower stresses (approx 200 MPa) at higher temperatures (approx 1000 °C) near the blade tips. Strengthening mechanisms in superalloys and single phase γ' have been recently reviewed by Pope and Ezz (ref. 2).

Temperature, strain rate, the sense of the applied stress, crystal orientation, and volume fraction and size of the γ' precipitates all have interesting effects on the flow stress of Ni-base superalloys. It has been observed that for some superalloys at temperatures less than about 800 °C, Schmid's law is not obeyed for orientations with the same octahedral slip system operating and that the deviation is asymmetric in tension and compression (refs. 3 to 5). Shah and Duhl (ref. 3) took the model of Lall, Chin, and Pope (ref. 6) for the flow stress behavior of single phase γ' based on a thermally activated cross slip model and extended it to account for γ' size effects in superalloy PWA 1480. The relationship between flow stress, strain rate, and deformation mode in [001]-oriented Mar-M200 single crystals has been shown by Leverant, et al. (ref. 7).

Only limited creep data on PWA 1480 have been published (refs. 8 and 9). More extensive studies have been reported for other single crystal superalloys (refs. 10 to 18). Some studies have concentrated heavily on the development

of the lamellar γ' morphology which forms in some alloys during creep at high temperatures (refs. 15 to 20). At slow rates of deformation and temperatures above 800 °C, the γ' particles coarsen directionally and develop into lamellar perpendicular to the axis of the applied tensile stress.

The present study is part of a larger program to understand the thermo-mechanical fatigue behavior of single crystal superalloys including the influence of the protective coatings used on turbine engine blades and vanes. Though considerable understanding exists of the simple mechanical behavior of single crystal superalloys and PWA 1480 in particular, it was necessary to obtain basic mechanical property data for the particular heat of PWA 1480 to be studied in the larger program. These data are presented for record herein, and it is shown how these data correspond to the established behavior for other lots of PWA 1480 and for other single crystal superalloys.

EXPERIMENTAL

Materials

The superalloy studied herein is designated PWA 1480 and was developed by Pratt and Whitney Aircraft for application as single crystal aircraft gas turbine blades and vanes (ref. 1). The alloy has the following nominal composition: 10Cr, 5Al, 1.5Ti, 12Ta, 4W, 5Co, balance Ni, in weight percent. The single crystal specimens were grown as round bars about 21 mm in diameter and 140 mm long. Bars having their [001] within 7° of the axis were selected for mechanical test specimens. These were heat treated before machining. After solution treatment for 4 hr at 1290 °C, the bars were aged at 1080 °C for 4 hr and then at 870 °C for 32 hr. ASTM standard tensile/creep test specimens of 6.3 mm diameter and 12.7 mm gauge length, and compression specimens of 5 mm diameter and 10 mm length were machined from the heat treated bars.

The microstructure of PWA 1480 is shown in figure 1. This alloy contains about 65 vol % of the γ'-phase, but essentially no carbides or borides. Since C, B, and Zr are not necessary for grain boundary strengthening in single crystals, they have not been employed in the PWA 1480 composition. Interdendritic porosity is known to be a problem in single crystal superalloys, and those studied herein were no exception. The crystals contained an average of about 0.3 vol % porosity. The pore diameter averaged about 7 μm with a standard deviation of about 6 μm. Considerable interdendritic γ' eutectic nodules were present in the crystals, about 1.5 vol %. Except in the interdendritic areas, the γ' precipitated in the solid state was cuboidal and uniform in size, averaging about 0.6 μm. In the interdendritic areas, which constituted about 7 percent of the alloy, the precipitated γ' was more irregular in shape and ranged in size from about 0.6 μm to about 3 times that size.

PROCEDURES

All tensile and compression tests were carried out on an Instron machine. An initial set of tensile tests were carried out over a wide range of temperatures (room temperature to 1200 °C) at a cross head speed of 0.02 in./min. Later tests were carried out in the 700 to 1050 °C temperature range over a

wide range of constant crosshead speeds. The strain rate was determined by dividing crosshead speed by the specimen gauge length.

To facilitate compression testing, the Instron machine was fitted with a superalloy compression gauge. The specimen was placed between superalloy pads lubricated with MoS_2 to reduce end constraint. Temperature was controlled in all tests to ±2 °C. The test data were recorded as load versus crosshead displacement, and plastic strain was obtained using the offset from the machine-specimen elastic loading line and the specimen gauge length.

Creep-rupture tests were carried out using constant load lever arms. Temperature was measured with two Pt/Pt-Rh thermocouples attached to the specimens and was controlled to ±2 °C. Creep strain was measured with a LVDT in conjunction with an extensometer attached to the shoulders of the specimen. Most of the tests were conducted to failure. A few tests were interrupted in the beginning of the second stage creep and cooled under load to examine by electron microscopy. A few constant load compressive tests were also carried at 1050 °C.

RESULTS

Flow Stress Behavior

The temperature dependence of tensile strength and ductility of PWA 1480 are shown in figures 2 and 3. It is clear in figure 2 that both yield and tensile strength increase with increase in temperature up to 700 °C and then drop sharply. The ductilities (elongation and reduction in area) remain low and nearly constant up to 700 °C and then increases with increasing temperature (fig. 3).

Figure 4 shows the yield strength of PWA 1480 as a function of temperature in unidirectional tension and compression. Clearly the material is stronger in tension than in compression for temperatures up to about 800 °C. This tension-compression asymmetry is most pronounced in the vicinity of 700 °C. Figure 4 also suggests that the temperature at which the sharp drop of the flow stress occurs is influenced by the sign of applied stress.

The dependence of the 0.2 percent offset flow stress (both tensile and compression) on strain rate is shown in figure 5 for five temperatures between 700 and 1050 °C. Several important effects should be noted. At 700 and 760 °C, the flow stress is independent of strain rate over the range 6.6×10^{-3} to $2 \times 10^{-1} s^{-1}$; and tension/compression anisotropy exists, tension being stronger than compression. A peak in strength is reached at a temperature near 800 °C for strain rates greater than about 10^{-2}. However, at this temperature flow stress decreases with decreasing strain rate. In tension, for strain rates less than about 10^{-2} the flow stress at 800 °C becomes less than that at 760 °C. Also, at 800 °C and strain rates greater than about 10^{-2}, the compressive flow stress appears to be higher than the tensile, unlike at lower temperatures. At 850 and 1050 °C, the flow stress again decreases with decreasing strain rate, and there appears to be little tension/compression asymmetry. In figure 6 the elongation at fracture, ε_f, is shown as a function of temperature for two strain rates.

CREEP BEHAVIOR

Tensile creep curves for single crystal PWA 1480 shown in figures 7(a) and (b) exhibit the three stages commonly observed for this type of material at high temperatures. Incubation periods were not observed at either test temperature. From each creep test, steady state creep rate, $\dot{\varepsilon}_s$, time to failure, t_f, time to the onset of tertiary creep, t_t, time to the onset of secondary creep, t_s, strain to the onset of secondary creep, ε_s, strain to onset of tertrary creep, ε_t, and total creep strain, ε_f, were obtained.

In figure 8 the secondary creep rates at 850 and 1050 °C are shown as a function of stress. Also shown are constant tensile flow stress values from the constant crosshead speed tests discussed previously. It may be seen that a power law relationship exists between strain rate and stress which extends from the region of the creep data connecting smoothly with the constant crosshead speed data up to strain rates of about 10^{-3} s^{-1}. The best fit equations for strain rate are $1.01 \times 10^{-40}\sigma^{12.2}$ and $1.59 \times 10^{-23}\sigma^{7.22}$ for 850 and 1050 °C, respectively. At the highest strain rates shown however, the power law behavior is seen to break down. Another interesting observation which confirmed that made previously during creep-fatigue tests of PWA 1480 (ref. 21), was that for a compression creep test the second stage creep rate was higher than for the test in tension at the same stress of 125 MPa. Creep rupture lives also had power law dependencies on the stress as shown in figure 9.

Many relationships between $\dot{\varepsilon}_s$ and rupture life, t_r, for constant load creep tests have been proposed. The most common form is that due to Monkman and Grant (ref. 22)

$$t_R \dot{\varepsilon}_s^a = c \tag{1}$$

with a and c being constant.

The logarithmic plot of $\dot{\varepsilon}_s$ versus t_r in PWA 1480 over a wide range of stress and temperature is shown in figure 10. Equation (1) fits the PWA 1480 combined data at 850 and 1050 °C with and R^2 of 94 percent.

Dobes and Milicka (ref. 23) modified equation (1) by introducing the strain to rupture, ε_R, to account for alloys exhibiting large tertiary creep
strains,

$$\left(\frac{t_r}{\varepsilon_R}\right) \dot{\varepsilon}_s^{a'} = c' \tag{2}$$

where a' and c' are constants.

Koul, et al. further modified equation (2) by eliminating time and strain in tertiary creep as follows (ref. 24).

$$\left(\frac{t_t}{\varepsilon_t}\right) \dot{\varepsilon}_s^b = K \tag{3}$$

Where b and K are constants. Neither equations (2) nor (3) provided any better correlation of the PWA 1480 creep data than did the Grant-Monkman equation.

CREEP FAILURE MODE

The fractured surface and the longitudinal sections of failed creep specimens were observed under optical and scanning electron microscopes. An SEM micrograph of a typical fractured surface of a specimen tested at 850 °C is shown in figure 11. Extensive crack nucleation and linkage of cracks at the micropores are evident.

Generally the fracture surfaces of specimens tested at 1050 °C were heavily oxidized and difficult to interpret. However, longitudinal sections of long-lived specimens tested at low stresses appeared to show cracks emanating from heavily oxidized surfaces (fig. 12). The needle-like phase in figure 12 is a complex oxide of titanium and tantalum. Necking also contributed to failure in low stress tests at both temperatures.

γ' MORPHOLOGY CHANGES DURING CREEP

The γ' morphology in the PWA 1480 prior to testing was cuboidal except in the interdendritic areas. In order to study the changes in γ' morphology after creep testing, specimens exposed at 850 and 1050 °C at various stress levels were examined under SEM.

At 850 °C, the γ' did not show any pronounced change in morphology during tensile creep. At 1050 °C, the γ' coarsened as irregular rafts perpendicular to the [001] stress axis. Microstructures of specimens tested at 1050 °C and 126 MPa are shown in figure 13. After 20 hr the γ' rafted structure is not fully developed (fig. 13(a)). After failure at 195 hr the γ' rafts have become considerably thicker and more irregular (fig. 13(b)). Even greater thickening of the γ' rafts at failure is evident in the specimen which failed after more than 5800 hr at 68 MPa shown in figure 14.

DISCUSSION

Flow Stress Behavior

The yield and ultimate tensile strengths for [001]-oriented PWA 1480 single crystals obtained here (fig. 2), are in good agreement with those reported by DeLuca and Cowles (ref. 8) and Swanson, et al. (ref. 9). The yield strengths reported by Shah and Duhl (ref. 3) are at least 10 percent higher at all temperatures, while those of Heredia and Pope (ref. 5) are significantly lower in the temperature regime of peak strength found by others. The higher strengths shown by Shah and Duhl may be explained by their having been able to fully dissolve all the γ' prior to aging, and/or a somewhat finer γ' size after aging. Complete dissolution of the γ' requires precise temperature control since the difference between the γ' solvus and solidus temperature is small for PWA 1480, and commercial heat treaters apparently do not risk melting parts. The commercially produced PWA 1480 crystals studied herein contained approximately 1.5 vol % of γ' present in undissolved eutectic nodules. The micrographs shown by DeLuca and Cowles, and Swanson, et al. exhibit γ' eutectic nodules like those present in the crystal studied here, however neither Shah and Duhl nor Heredia and Pope present any micrographs.

Differences among investigations may also arise from differences in the size of the γ' precipitates. Shah and Duhl showed that for temperatures below about 700 °C, yield strength increases dramatically with decreasing γ' size. The most comparable data from their work correspond to a γ' size of 0.5 μm which is slightly finer than the 0.6 μm size in the crystals studied here. Heredia and Pope, however, report an even finer γ' size, and their crystals were the weakest of all. Of the two studies showing yield strengths similar to those reported here, DeLuca and Cowles show what appears to be a comparable γ' size, but Swanson, et al. report a very large γ' size, 0.9 μm.

The temperature dependence of the flow stress of PWA 1480 is typical of superalloys containing a high volume fraction of the γ' phase (ref. 2). At temperatures up to 600 °C, the flow stress appears nearly constant. However, Shah and Duhl also tested at 400 °C and found a dip in the flow stress at that temperature (ref. 3). For temperatures above about 600 °C the flow stress increases with temperature, reaches a peak at about 700 °C, and then decreases. The increasing flow stress with increasing temperature is attributed to thermally activated locking of the a/2 <110> dislocation pairs which must shear the ordered γ' phase. For crystal orientations other than [001], the peak in flow stress may be explained by the onset of primary cube slip. However, for [001]-oriented crystals the resolved shear stress on the primary cube planes is very low, and the peak in flow stress is more likely explained by a 'saturation stress' concept (ref. 2). At low temperatures the strength of the locking mechanism is very great but only a small fraction of the dislocations are immobilized. Flow stress increases with temperature due to the decreased fraction of mobile dislocations. However, the strength of the locking mechanism decreases with temperature, and above some temperature it no longer influences the flow stress.

The elongations to fracture of the crystals studied here, figure 2, are the same at room temperature and temperatures around 1000 °C as those reported by others (refs. 8 and 9). However, elongations are reported for the regime of 700 to 800 °C which are about twice those measured here. The reason for this difference in behavior is not known.

TENSION/COMPRESSION ANISOTROPY

It is important to note in figure 4 that flow stress strongly depends on the sense of applied stress for [001]-oriented specimens in the vicinity of 700 °C with the tensile flow stress exceeding the compressive flow stress. The tension/compression anisotropy has been explained by the model of Lall, Chin, and Pope (refs. 2 and 6) and its refinement in terms of dislocation core dissociation in the γ' phase by Paidar, Pope, and Viteck (refs. 2 and 25). The temperature at which the flow stress reaches a peak value is also influenced by the sign of the applied stress. It is clear in figure 4 that the peak stress temperature for tension was lower than that for compression. A similar observation was made by Heredia and Pope (ref. 5) and by Ezz (ref. 26) for [001]-oriented single crystal $Ni_3(Al,Nb)$.

STRAIN-RATE EFFECTS ON FLOW STRENGTH

In figure 5 two types of behavior can be observed for the strain-rate dependence of the flow stress. A strain rate independent flow stress was found at 700 and 760 °C in the strain range of $6x10^{-4}$ to $2x10^{-1}$ sec^{-1}, and a strain rate dependent flow stress at 800 °C and above. Leverant, et al. (ref. 7) determined the temperature and strain rate dependence of the compressive 0.1 percent offset yield stress in [001]-oriented Mar-M 200 single crystals as shown in figure 15. PWA 1480 and Mar-M 200 behave almost identically, except that the transition temperature is lower in PWA 1480.

Note that for both Mar-M 200 and PWA 1480 at high strain rates, flow stress peaks at some temperature greater than 760 °C, and the increase in flow stress above that at 760 °C increases with increasing strain rate, at least until some limit is reached. It is also apparent that the range of temperatures over which the flow stress exceeds that for 760 °C increases with increasing strain rate.

Leverant, et al. summarized the microscopic evidence on the deformation mechanisms of Mar-M 200 follows. The low temperature, strain rate independent flow stress is controlled by diffusionless shear of the γ' precipitates by a/2 <110> dislocation pairs in coarse planar bands. The high temperature, strain rate dependent flow stress is controlled by a more homogeneous distribution of dislocations both of the a/2 <110> and a/3 <112> type which shear the γ' by a diffusion controlled viscous glide process.

Though the low temperature shearing mechanism by a/2 <110> dislocation pairs is strain rate independent, increasing strain rate does increase the upper temperature limit to which it operates. Also, as the upper temperature limit increases so does the strength at that temperature because of the thermally activated strengthening mechanism. Thus, both the peak strength and corresponding temperature increase with increasing strain rate. Decreasing strain rates have the opposite effect by lowering the temperature at which diffusion controlled glide mechanisms begin to operate.

The lack of strain rate sensitivity for the low temperature shearing mechanism in the γ' appears to be inconsistent with the cube cross slip locking mechanism of Takeuchi and Kuramoto (ref. 27) incorporated into subsequent models (refs. 6 and 27), since a higher strain rate requires a higher dislocation velocities and therefore allows less time for the formation of cross slipped segments. Pope and Ezz (ref. 2) propose that this inconsistency can be resolved if it is assumed that dislocations can also penetrate the obstacles at cross-slipped segments by a thermally activated process. The strain rate sensitivity is then the sum of a negative term representing the formations of cross-slipped segments, and a positive term representing the thermally activated penetration of the segments. Thus the sum of these two terms yields a small positive strain rate sensitivity.

CREEP BEHAVIOR OF PWA 1480

For the stress levels employed, PWA 1480 did not exhibit an incubation period for creep either at 1050 or 850 °C (figs. 7(a) and (b)), respectively. At temperatures below about 800 °C, an incubation period for creep is common

for single crystal superalloys (refs. 10, 14, and 15), however at about 850 °C and above observation of incubation periods are rare (ref. 16). The incubation period has been tied to the low initial density of dislocations, and high drag stress in the single crystal superalloys (ref. 10). The disappearance of the incubation period at higher temperatures can be attributed to the reduction in drag stress, increasing dislocation velocity, and possibly to the punching out of additional dislocations at the γ-γ' interface in alloys with large lattice parameter mismatch between γ and γ' (ref. 16).

GAMMA PRIME STABILITY

The high temperature creep resistance of some single crystal superalloys is greatly increased by the coarsening of the γ' to form continuous lamellea, or "rafts." Under tensile creep loading these rafts form perpendicular to the stress axis if the lattice parameter of the γ' is less than that of the γ phase, which is defined as negative mismatch. Recent studies have shown that creep resistance is maximized by the development of fine, perfectly continuous γ' rafts (refs. 15 and 18). Rapid development of such fine, highly perfect rafts early in second stage creep is promoted by large negative γ-γ' lattice mismatch at the temperature of creep exposure (ref. 20), and a fine initial γ' size (ref. 18).

The γ' rafts developed in the PWA 1480 studied here were not as perfect as those shown in some other alloys (refs. 16 to 20). The γ-γ' lattice parameter mismatch of PWA 1480 has not been measured, but appears to be close to zero (ref. 28), although the orientation of the rafts indicates that the mismatch is negative at the testing temperature.

SUMMARY OF RESULTS

Tensile and compression tests at temperatures from room temperature to 1200 °C at various strain rates and constant load creep tests at 850 and 1050 °C were performed on single crystal of the nickel-base superalloy PWA 1480 with [001] orientation. Tensile/compressive yield strengths were compared with respect to their dependence on temperature and strain rates. Creep behavior of PWA 1480 were studied in terms steady state creep rate, time to rupture and microstructural features. The following results were obtained:

1. The flow stress of [001]-oriented PWA 1480 increased with increasing temperature above ambient but began to decrease markedly above 760 to 800 °C. For temperatures less than about 760 °C, flow stress was insensitive to strain rate and the tensile flow stress markedly exceeded that for compressive flow at 700 and 760 °C.

2. At 800 °C and above, the flow stress of [001]-oriented PWA 1480 decreased continuously with decreasing strain rate. However, at the highest strain rates the flow stress continued to increase with temperature to about 800 °C, and particularly the compressive flow stress, which became higher than the tensile flow stress. At lower strain rates and higher temperatures the tension/compression anisotropy diminished.

3. The steady state creep rate and time to failure exhibited power law dependencies on applied stress. The stress exponents were 7.2 and 12.2 for 1050 and 850 °C, respectively.

4. During creep at 1050 °C, directional coarsening of γ' was very prominent for all stress levels, however directional coarsening of γ' was not evident in the specimens crept at 850 °C. Considerable surface oxidation was observed on the long lived specimens tested at lower applied stresses.

REFERENCES

1. Gell, M.; Duhl, D.N.; and Giamai, A.F.: The Development of Single-Crystal Super-Alloy Turbine-Blades. Superalloys 1980, J.K. Tien, et al., eds., American Society for Metals, Metals Park, OH, 1980, pp. 205-214.

2. Pope, D.P.; and Ezz, S.S.: Mechanical Properties of Ni_3Al and Nickel-Base Alloys with High Volume Fraction of γ': Int. Met. Rev., vol. 29, no. 3, 1984, pp. 136-167.

3. Shah, D.M.; and Duhl, D.M.: The Effect of Orientation, Temperature and Gamma-Prime Size on the Yield Strength of a Single-Crystal Nickel-Base Superalloy. Superalloys 1984, M. Gell, et al., eds., TMS-AIME, Warrendale, PA, 1984, pp. 105-114.

4. Miner, R.V.; Gayda, T.P.; and Hemker, K.J.: Orientation and Temperature Dependence of Some Mechanical Properties of the Single-Crystal Nickel-Base Superalloy RENE N4: III. Tension-Compression Anisotropy. Metall. Trans. A, vol. 17, no. 3. Mar. 1986. pp. 507-512.

5. Heredia, F.E.; and Pope, D.P.: The Tension/Compression Flow Asymmetry in a High γ' Volume Fraction Nickel Base Alloy. Acta Met., vol. 34, no. 2, Feb. 1986, pp. 279-285.

6. Lall, C.; Chin, S.; and Pope, D.P.: The Orientation Temperature Dependence of the Yield Stress of $Ni_3(Al,Nb)$ Single Crystals. Metall. Trans. A, vol. 10, no. 9, Sept. 1979, pp. 1323-1332.

7. Leverant, G.R.; Gell, M.; and Hopkins, S.W.: The Effect of Strain Rate on the Flow Stress and Dislocation Behavior of a Precipitation-Hardened Nickel-Base Alloy. Mater. Sci. Eng., vol. 8, 1971, pp. 125-133.

8. Deluca, D.P.; and Cowles, B.A.: Fatigue and Fracture of Advanced Blade Materials. AFWAL-TR-84-4167, Air Force Wright Aeronautical Laboratories, Wright-Patterson Air Force Base, Feb. 1985. (AD-B095265L)

9. Swanson, G.A., et al.: Life Prediction and Constitutive Models for Engine Hot Section Anisotropic Materials Program. (PWA-5968-19, Pratt and Whitney Aircraft; NASA Contract NAS 3-23939) NASA CR-174952, 1986.

10. Leverant, G.R.; and Kear, B.H.: The Mechanism of Creep in Gamma Prime Precipitation-Hardened Nickel-Base Alloys at Intermediate Temperatures. Metall. Trans., vol. 1, no. 2, Feb. 1970, pp. 491-498.

11. Leverant, G.R.; Kear, B.H.; and Oblak, J.M.: Creep of Precipitation-Hardened Nickel-Base Alloy Single Crystals at High Temperatures. Metall. Trans., vol. 4, no. 1, Jan. 1973, pp. 355-362.

12. Cary, C.; and Strudel, J.L.: Apparent and Effective Creep Parameters in Single Crystals of a Nickel Base Superalloy-II. Secondary Creep. Acta Met., vol. 26, no. 5, May 1978, pp. 859-870.

13. MacKay, R.A.; Dreshfield, R.L.; and Maier, R.D.: Anisotropy of Nickel-Base Super-Alloy Single-Crystals. Superalloys 1980, J.K. Tien, et al., eds., ASM, Metals Park, OH, 1980, pp. 385-394.

14. MacKay, R.A.; and Maier, R.D.: The Influence of Orientation on the Stress Rupture Properties of Nickel-Base Superalloy Single Crystals. Metall. Trans. A, vol. 13, no. 10, Oct. 1982, pp. 1747-1754.

15. Caron, P.; and Khan, T.: Improvement of Creep Strength in a Nickel-Base Single-Crystal Superalloy by Heat Treatment. Mater. Sci. Eng., vol. 61, no. 2, Nov. 1983, pp. 173-184.

16. Nathal, M.V.; and Ebert, L.J.: Elevated Temperature Creep-Rupture Behavior of the Single Crystal Nickel-Base Superalloy NASAIR 100. Metall. Trans. A., vol. 16, no. 3, Mar. 1985, pp. 427-439.

17. Nathal, M.V.; and Ebert, L.J.: The Influence of Cobalt, Tantalum, and Tungsten on the Elevated Temperature Mechanical Properties of Single Crystal Nickel-Base Superalloys. Metall. Trans. A, vol. 16, no. 10, Oct. 1985, pp. 1863-1870.

18. MacKay, R.A.: and Ebert, L.J.: Factors Which Influence Directional Coarsening of Gamma-Prime During Creep in Nickel-Base Superalloy Single-Crystals. Superalloys 1984, M. Gell, et al., eds., TMS-AIME, Warrendale, PA, 1984, pp. 135-144.

19. Pearson, D.D.; Lemkey, F.D.; and Kear, B.H.: Stress Coarsening of Gamma Prime and Its Influence on Creep-Properties of a Single-Crystal Super-Alloy. Superalloys 1980, J.K. Tien, et al., eds., ASM, Metals Park, OH, 1980, pp. 513-520.

20. Nathal, M.V,; MacKay, R.A.; and Garlick, R.G.: Temperature Dependence of γ-γ' Lattice Mismatch in Nickel-Base Superalloys. Mater. Sci. Eng., vol. 75, 1985, pp. 195-205.

21. Miner, R.V.; Gayda, J.; and Hebsur, M.G.: Creep-Fatigue Behavior of NiCoCrAlY Coated PWA 1480 Superalloy Single Crystals. NASA TM-87110, 1985.

22. Monkman, F.C.; and Grant, N.J.: An Empirical Relationship Between Rupture Life and Minimum Creep Rate in Creep-Rupture Tests. Proc. ASTM, vol. 56, 1956, pp. 593-620.

23. Dobes, F.; and Milicka, K.: The Relation Between Minimum Creep Rate and Time to Fracture. Met. Sci., vol. 10, Nov. 1976, pp. 382-384.

24. Koul, A.K.; Castillo, R.; and Willett, K.: Creep Life Predictions in Nickel-Based Superalloys. Mater. Sci. Eng., vol. 66, 1984, pp. 213-226.

25. Paidar, V.; Pope, D.P.; and Vitek, V.: A Theory of the Anomalous Yield Behavior in $L1_2$ Ordered Alloys. Acta Met., vol. 32, no. 3, Mar. 1984, pp. 435-448.

26. Ezz, S.S.: Plastic Flow Asymmetry and Dislocation Core Structure in $L1_2$ Ordered Alloy Crystals. PhD Thesis, Univ. of Pennsylvania, 1984.

27. Takeuchi, S.; and Kuramoto, E.: Temperature and Orientation Dependence of the Yield Stress in Ni_3Ga Single Crystals. Acta Met., vol. 21, No. 4, Apr. 1973, pp. 415-425.

28. MacKay, R.A.; and Garlick, R.G.: Unpublished research.

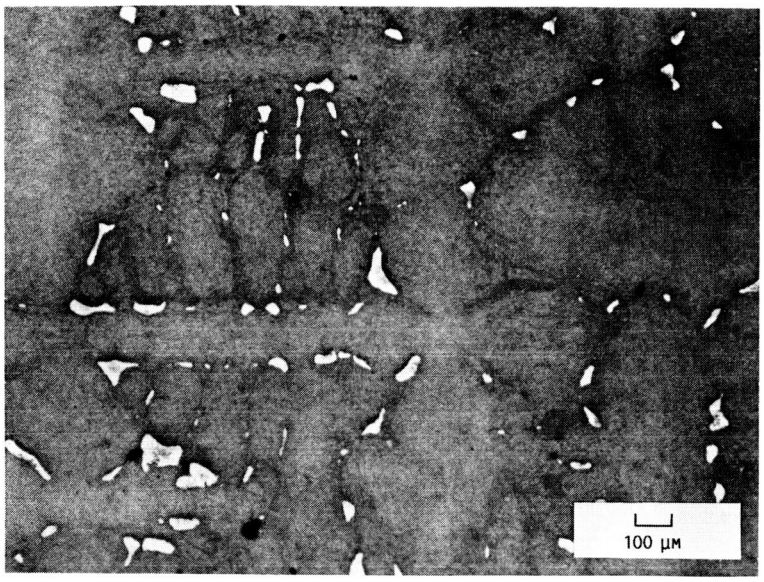

(A) SHOWING INTERDENTRIDIC γ′ EUTECTIC NODULES AND POROSITY.

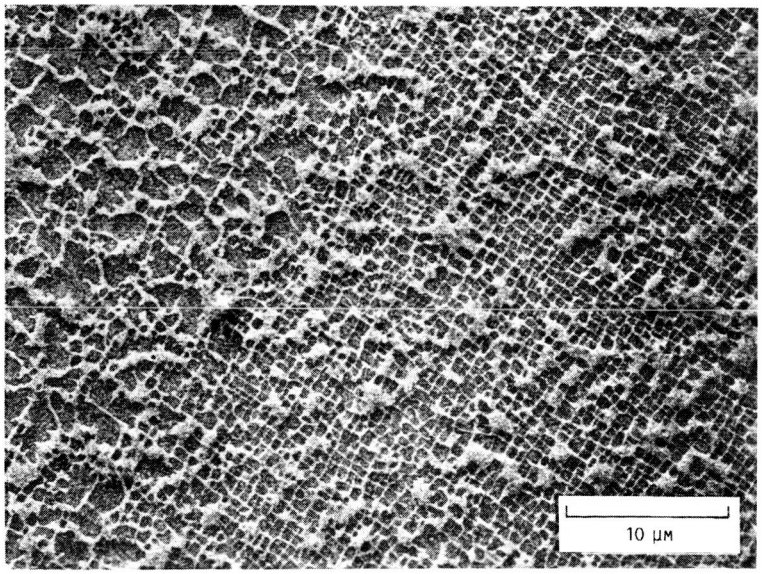

(B) DETAIL SHOWING COARSENED γ′ IN INTERDENTRIDIC AREA CONTRASTED WITH "NORMAL" γ′.

FIGURE 1. - MICROSTRUCTURE OF PWA 1480.

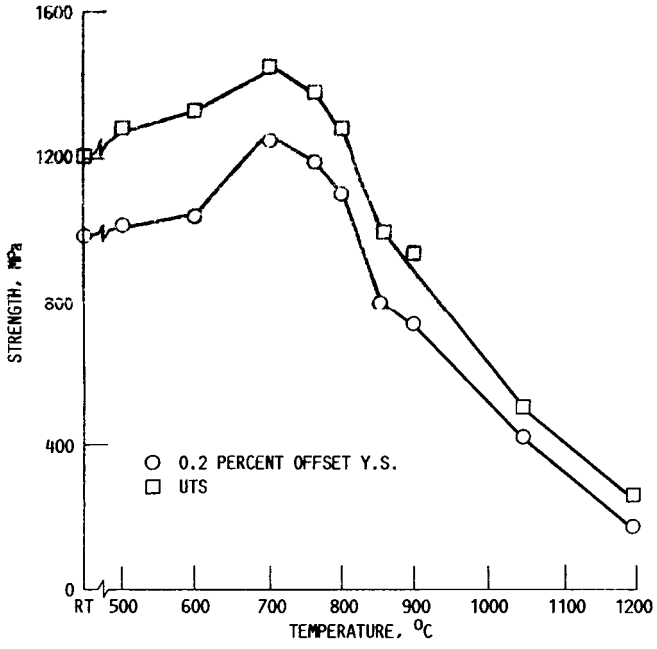

FIGURE 2.- TENSILE YIELD AND ULTIMATE STRENGTHS AS A FUNCTION OF TEMPERATURE FOR [001]-ORIENTED PWA 1480, STRAIN RATE, $\dot{\varepsilon}$, 6.6×10^{-4} s^{-1}.

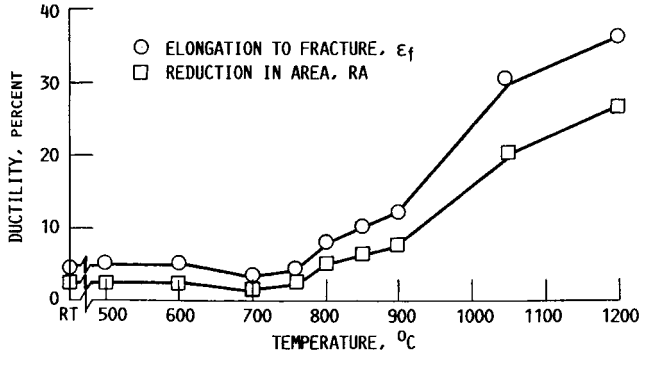

FIGURE 3.- DUCTILITY AS A FUNCTION OF TEMPERATURE FOR [001]-ORIENTED PWA 1480. STRAIN RATE, $\dot{\varepsilon}$, 6.6×10^{-4} s^{-1}.

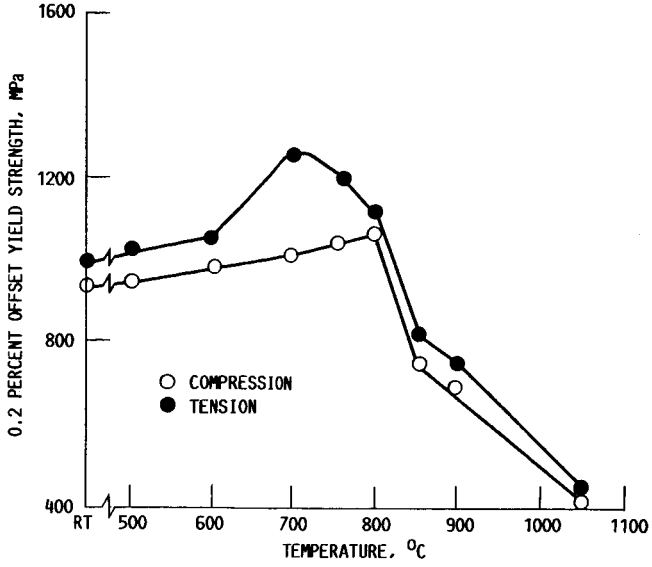

FIGURE 4.- FLOW STRESS AS A FUNCTION OF TEMPERATURE AND SENSE OF APPLIED STRESS FOR [001]-ORIENTED PWA 1480. STRAIN RATE, $\dot{\varepsilon}$, 6.6×10^{-4} s^{-1}.

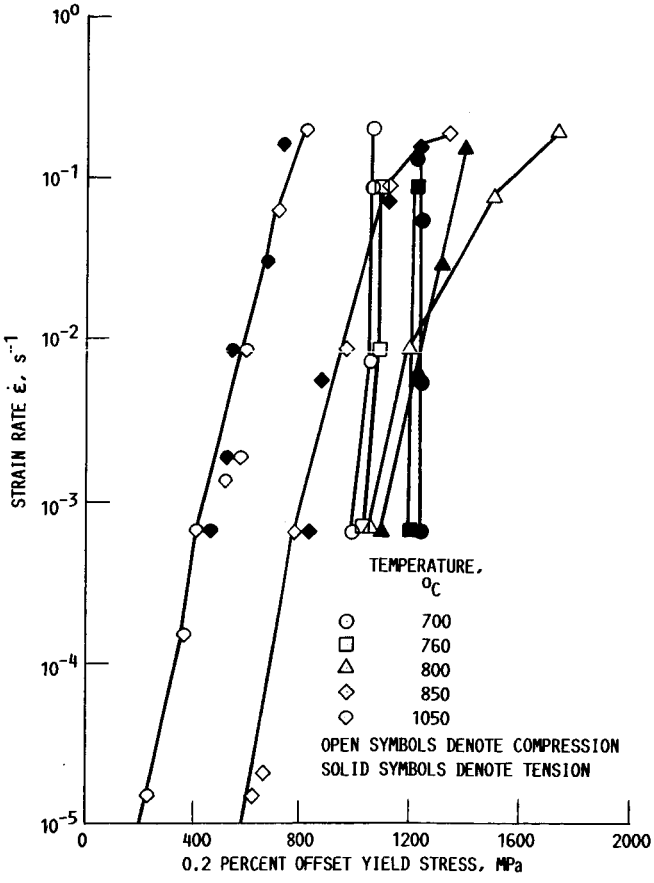

FIGURE 5.- YIELD STRESS AS A FUNCTION OF TEMPERATURE, STRAIN RATE, AND SENSE OF APPLIED STRESS FOR [001]-ORIENTED PWA 1480.

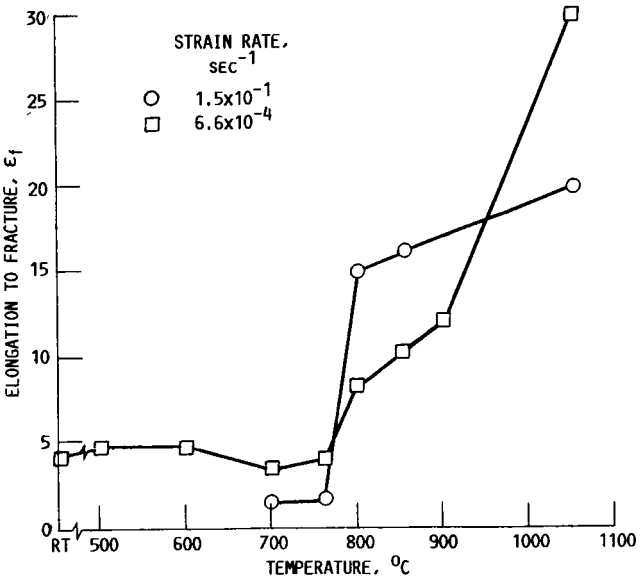

FIGURE 6.- ELONGATION TO FRACTURE IN STRESS-STRAIN TESTING AS A FUNCTION OF TEMPERATURE, SHOWING A DUCTILITY MINIMUM, FOR [001]-ORIENTED PWA 1480.

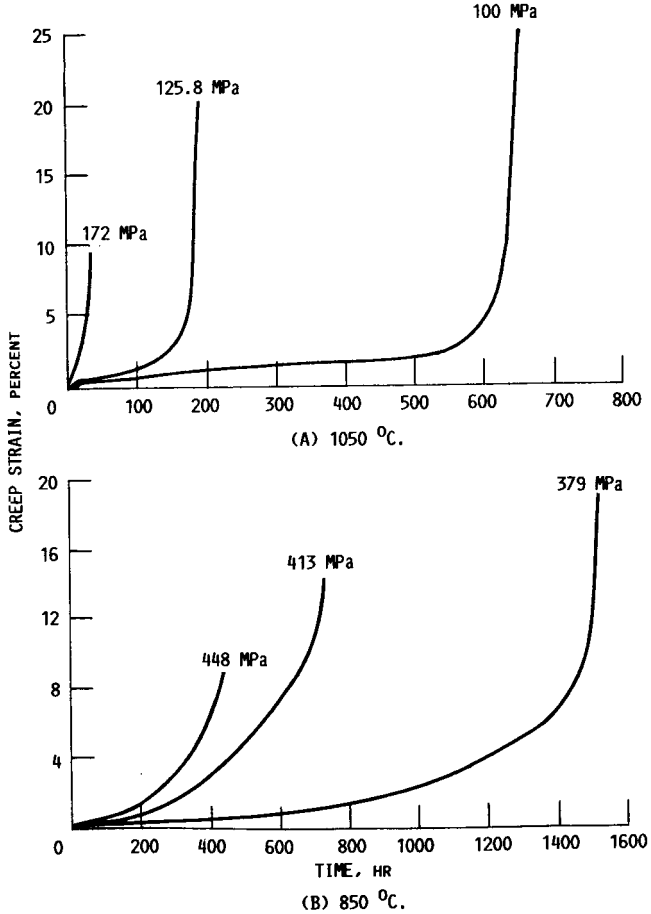

FIGURE 7.- TYPICAL CREEP CURVES FOR [001]-ORIENTED PWA 1480.

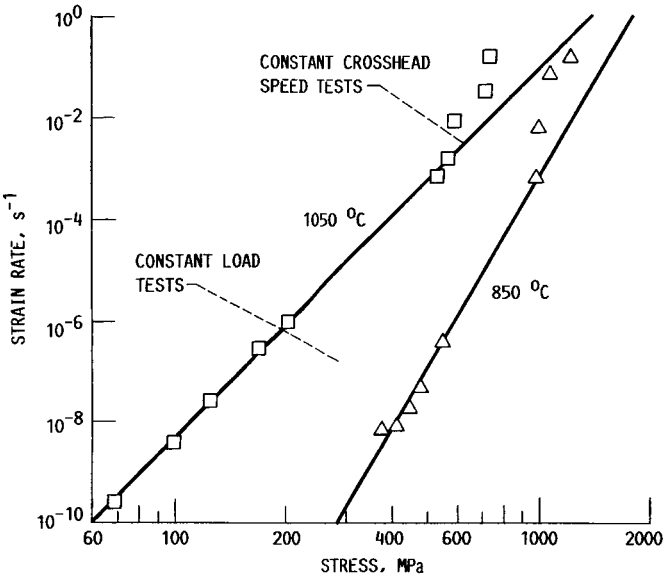

FIGURE 8.- FLOW STRESS BEHAVIOR OF PWA 1480.

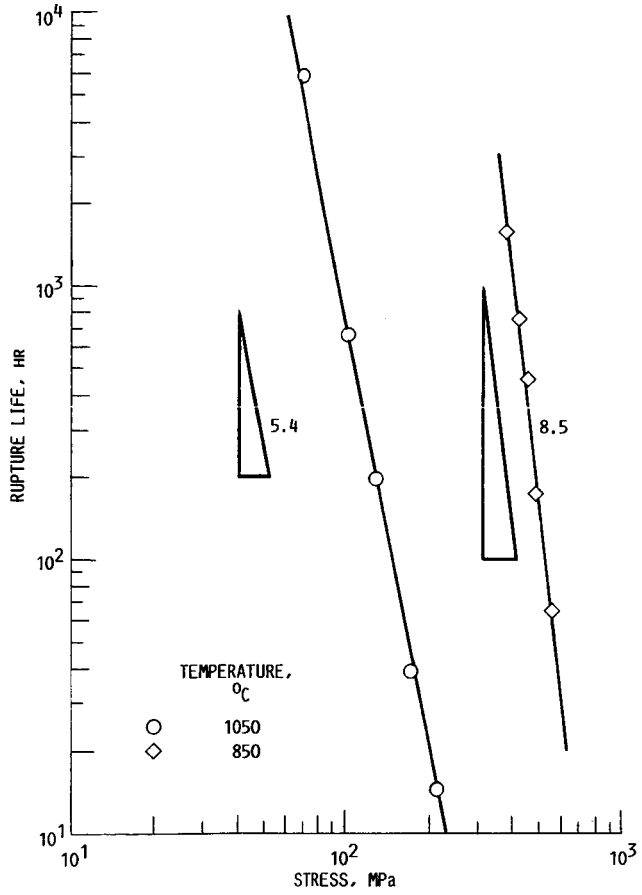

FIGURE 9.- STRESS DEPENDENCE OF CREEP RUPTURE LIFE AS A FUNCTION OF APPLIED STRESS FOR PWA 1480 AT 850 °C AND 1050 °C.

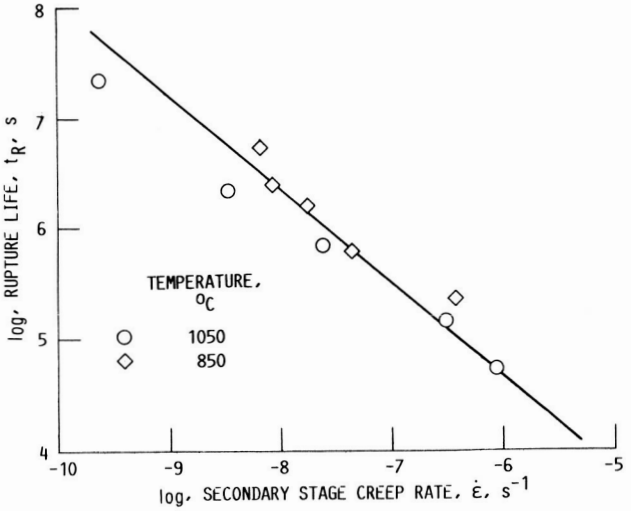

FIGURE 10. - RUPTURE LIFE AS A FUNCTION OF CREEP REATE FOR PWA 1480 BASED ON MONKMAN-GRANT RELATIONSHIP, $\log t_R = 0.59 - 0.712 \log \dot{\epsilon}$. R^2 = 93.5 PERCENT; S.D. = 0.2.

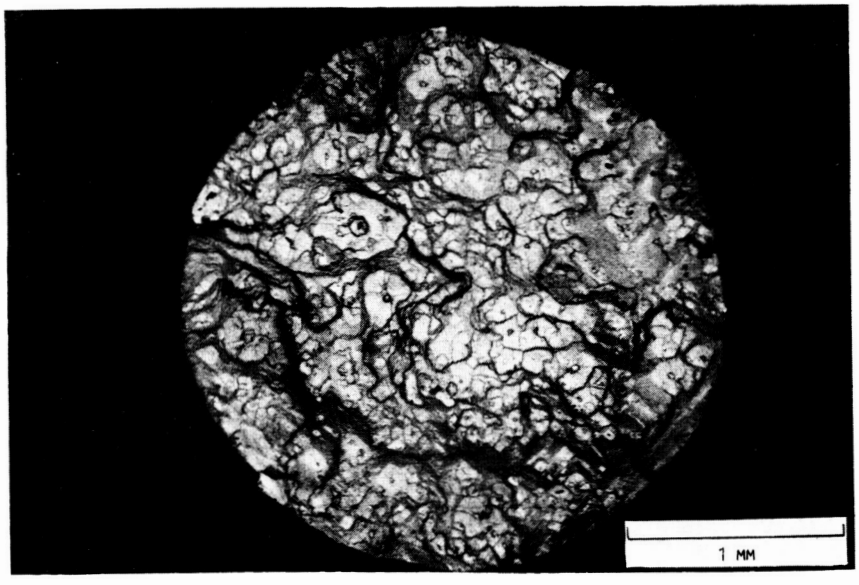

FIGURE 11. - SEM MICROGRAPH OF PWA 1480 SPECIMEN FRACTURED AT 410 MPA AND 850 °C, ILLUSTRATING MULTIPLE INTERNAL CRACK INITIATION AT MICROPORES.

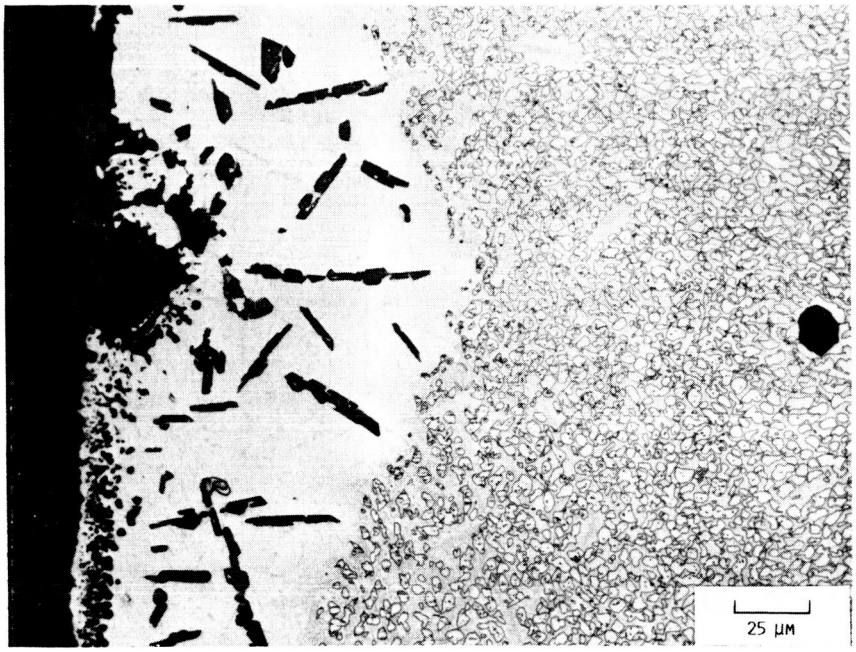

FIGURE 12. - OPTICAL MICROGRAPH OF LONGITUDINAL SECTION OF PWA 1480 SPECIMEN TESTED AT 1050 °C AND 68 MPa, INDICATING THE HEAVILY OXIDIZED SURFACE.

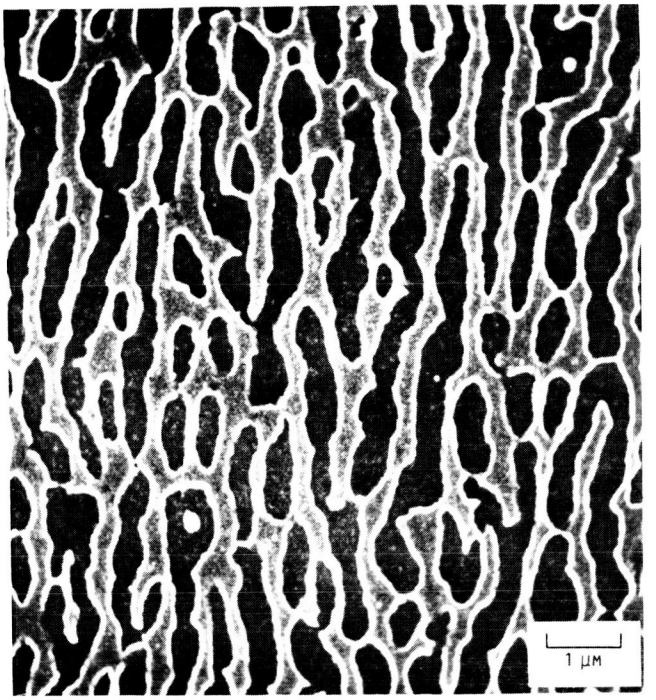

(A) FOR 20 HOURS.

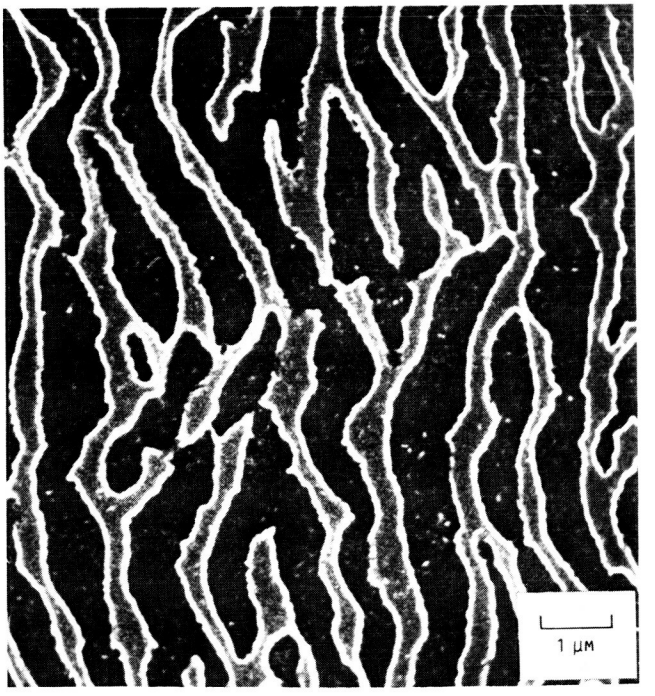

(B) AFTER FAILURE AT 194.5 HOURS.

FIGURE 13. - LONGITUDINAL MICROSTRUCTURES OF SAMPLES TESTED AT 1050 ^{o}C AND 126 MPa. (STRESS AXIS IS HORIZONTAL)

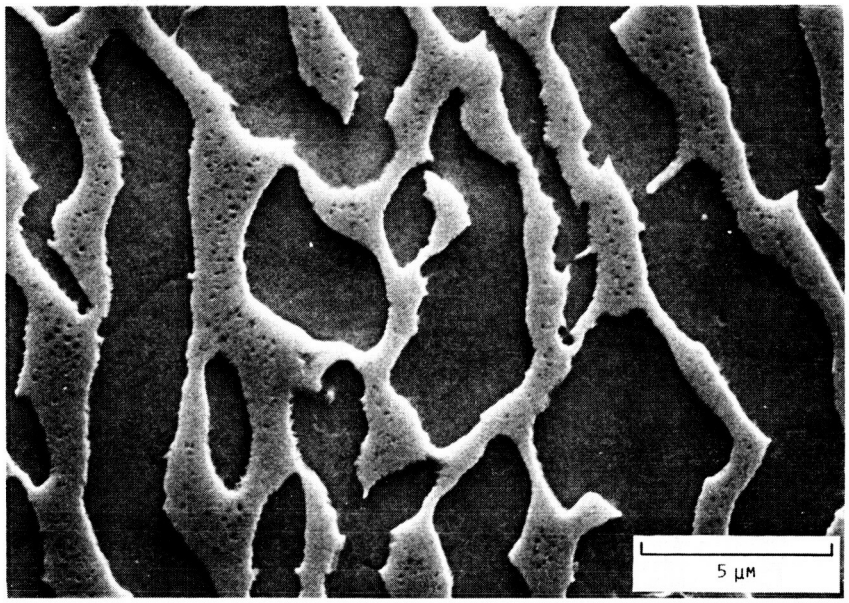

FIGURE 14. - GAMMA PRIME (γ') DIRECTIONAL COARSENING IN PWA 1480 SPECIMEN FAILED AFTER 5800 HOURS AT 1050 ^{o}C AND 68 MPa. (STRESS AXIS IS HORIZONTAL)

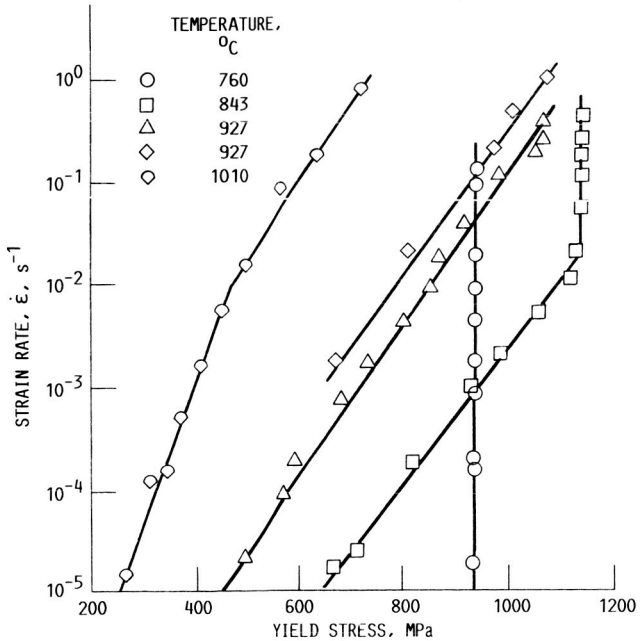

FIGURE 15.- YIELD STRESS AS A FUNCTION OF STRAIN RATE AND TEMPERATURE FOR [001]-ORIENTED MAR-M 200. (FROM REF. 5.)

1. Report No.	2. Government Accession No.	3. Recipient's Catalog No.
NASA TM-88950		

4. Title and Subtitle	5. Report Date
Elevated Temperature Tension, Compression, and Creep-Rupture Behavior of [001]-Oriented Single Crystal Superalloy PWA 1480	February 1987
	6. Performing Organization Code: 505-63-01
7. Author(s): Mohan G. Hebsur and Robert V. Miner	8. Performing Organization Report No.: E-3074
	10. Work Unit No.
9. Performing Organization Name and Address: National Aeronautics and Space Administration, Lewis Research Center, Cleveland, Ohio 44135	11. Contract or Grant No.
	13. Type of Report and Period Covered: Technical Memorandum
12. Sponsoring Agency Name and Address: National Aeronautics and Space Administration, Washington, D.C. 20546	14. Sponsoring Agency Code

15. Supplementary Notes

16. Abstract

Tensile and compressive flow behavior at various temperatures and strain rates, and tensile creep rupture behavior at 850 and 1050 °C and various stresses were studies for [001]-oriented single crystals of the Ni-base superalloy PWA 1480. At temperatures up to 760 °C, the flow stress is insensitive to strain rate and of greater magnitude in tension than in compression. At temperatures of 800 °C and above, the flow stress decreases continuously with decreasing strain rate and the tension/compression anisotropy diminishes. The second stage creep rate and rupture time exhibited power law relationships with the applies stress for both 850 and 1050 °C, however with different stress dependencies. The stress exponent for the steady state creep rate was about 7 at 1050 °C, but much higher at 850 °C, about 12. Directional coarsening of the γ' phase occurred during creep at 1050 °C, but not at 850 °C.

17. Key Words (Suggested by Author(s))	18. Distribution Statement
Single crystal superalloy; Flow stress; Strain rate effects; Directional coarsening; Tension/compression anisotropy	Unclassified - unlimited STAR Category 26

19. Security Classif. (of this report)	20. Security Classif. (of this page)	21. No. of pages	22. Price*
Unclassified	Unclassified		

*For sale by the National Technical Information Service, Springfield, Virginia 22161